

Aeolian sediment fingerprinting using a Bayesian mixing model

Journal:	<i>Earth Surface Processes and Landforms</i>
Manuscript ID	ESP-17-0002.R1
Wiley - Manuscript type:	Research Article
Date Submitted by the Author:	n/a
Complete List of Authors:	Gholami, Hamid; University of Hormozgan, Department of Range and Watershed Management Telfer, Matt; Plymouth University, School of Geography, Earth and Environmental Sciences Blake, William; Plymouth University, SoGEES Fathabadi, Abolhassan; University of Gonbad-e-Kavoos, Department of Range and Watershed Management
Keywords:	Aeolian sediment, Sand provenance, Markov Chain Monte Carlo, Fingerprinting, Dune

SCHOLARONE™
Manuscripts

1 **Aeolian sediment fingerprinting using a Bayesian mixing model**

2
3 Hamid Gholami ^{a*}, Matt W. Telfer ^{b*}, William H. Blake ^b and Abolhassan Fathabadi ^c

4 ^a Department of Range and Watershed Management, University of Hormozgan,
5 Bandar-Abbas, Hormozgan, Iran.

6 ^b School of Geography, Earth and Environmental Sciences, Plymouth University,
7 Plymouth, Devon, PL4 8AA , UK.

8 ^c Department of Range and Watershed Management, University of Gonbad-e-
9 Kavoos, Gonbad-e-Kavoos, Golestan, Iran.

10 * Correspondence to:

11 Hamid Gholami, Department of Range and Watershed Management, University of
12 Hormozgan, Bandar-Abbas, Hormozgan, Iran. *E-mail address:*
13 hgholami@hormozgan.ac.ir. Tel: +98 937 0865077.

14 and

15 Matt Telfer, School of Geography, Earth and Environmental Science, Plymouth
16 University, Plymouth, Devon, PL4 8AA, UK. *E-mail address:*
17 matt.telfer@plymouth.ac.uk. Tel: +44 1752 585570.

18 19 **Abstract**

20 Identifying sand provenance in depositional aeolian environments (e.g. dunefields)
21 can elucidate sediment pathways and fluxes, and inform potential land management
22 strategies where windblown sand and dust is a hazard to health and infrastructure.

1
2
3 23 However, the complexity of these pathways typically makes this a challenging
4
5 24 proposition, and uncertainties on the composition of mixed-source sediments are
6
7 25 often not reported. This study demonstrates that a quantitative fingerprinting method
8
9
10 26 within the Bayesian Markov Chain Monte Carlo (MCMC) framework offers great
11
12 27 potential for exploring the provenance and uncertainties associated with aeolian
13
14 28 sands.

15
16 29 Eight samples were taken from dunes of the small (~58 km²) Ashkzar erg, central
17
18 30 Iran, and forty-nine from three distinct potential sediment sources from the
19
20 31 surrounding area. These were analyzed for 61 tracers including 53 geochemical
21
22 32 elements (trace, major and rare earth elements (REE)) and 8 REE ratios. Kruskal–
23
24 33 Wallis H-tests and stepwise discriminant function analysis (DFA) allowed the
25
26 34 identification of an optimum composite fingerprint based on six tracers (Rb, Sr, ⁸⁷Sr,
27
28 35 (La/Yb)_n, Ga and δCe), and a Bayesian mixing model was applied to derive the
29
30 36 source apportionment estimates within an uncertainty framework.

31
32
33
34 37 There is substantial variation in the uncertainties in the fingerprinting results, with
35
36 38 some samples yielding clear discrimination of components, and some with less clear
37
38 39 fingerprints. Quaternary terraces and fans contribute the largest component to the
39
40 40 dunes, but they are also the most extensive surrounding unit; clay flats and marls,
41
42 41 however, contribute out of proportion to their small outcrop extent. The successful
43
44 42 application of these methods to aeolian sediment deposits demonstrates their
45
46 43 potential for providing quantitative estimates of aeolian sediment provenances in
47
48 44 other mixed-source arid settings, and may prove especially beneficial where
49
50 45 sediment is derived from multiple sources, or where other methods of provenance
51
52 46 (e.g. detrital zircon U-Pb dating) are not possible due to mineralogical constraints.
53
54
55
56
57
58
59
60

1
2
3
4
5
6
7
8
9
10
11
12
13
14
15
16
17
18
19
20
21
22
23
24
25
26
27
28
29
30
31
32
33
34
35
36
37
38
39
40
41
42
43
44
45
46
47
48
49
50
51
52
53
54
55
56
57
58
59
60

47 **Key words:** Sand provenance; Aeolian sediment; Markov Chain Monte Carlo;
48 Fingerprinting; uncertainty.

For Peer Review

1. Introduction

Identifying and quantifying the source(s) of aeolian sediments is a long-standing challenge for geoscientists, and yet such information is often of crucial importance in understanding sediment fluxes at a range of scales. As well as providing fundamental knowledge on long-term landscape evolution (e.g. Pell et al., 1997), aeolian provenance studies have been used to elucidate past wind regimes and palaeoclimates (e.g. Nanson et al., 1995), investigate hazardous dust transport pathways (e.g. Pethierick et al., 2008; Yang et al., 2007) and inform studies of the palaeoclimatic record of the Antarctic ice-core dust record (Delmonte et al., 2010; Delmonte et al., 2004). The challenges with the task arise not just from the diverse range of potential sources for aeolian sands and dusts (e.g. geological or lithological units, soil units, land use types and geomorphological landscapes), and the long transport distances which may be involved (on the order of $10\text{-}10^2$ km for aeolian sand and $10\text{-}10^3$ km for aeolian dust), but also the potential complexity of transport pathways (Huntsman-Mapila et al., 2005). Before deposition at its current location, an aeolian sand grain may have been through multiple cycles of fluvial, aeolian, lacustrine and/or colluvial deposition and subsequent mobilization. Aeolian sands, therefore, rarely retain an easy-to-interpret signature of their origins.

The use of geochemical fingerprinting methods to determine sediment provenance has progressively increased since the late 1990s (Walling, 2013). Application has been focused most widely in fluvial contexts (Haddadchi et al 2013) wherein there recent work has highlighted the need to pay attention to challenges in signature development and tracer behavior (Koiter et al., 2013). Sediment fingerprinting involves the identification, quantification and statistical testing of a range of source

1
2
3 74 material properties capable of discriminating between potential sediment sources
4
5 75 with a view to improving knowledge of sediment source and transport processes
6
7 76 (Collins et al., 2017) . These properties may include geochemical characteristics
8
9 77 (e.g. Douglas et al., 2009; Lin et al., 2015), radionuclide concentrations (Wilson et
10
11 78 al., 2012), mineralogy (Pittam et al., 2009), geochronological data (principally U-Pb
12
13 79 dating of detrital zircons; e.g. Pell et al., 1997; Garzanti et al., 2013), biomarkers
14
15 80 (Chen et al., 2016) and colour properties (Martínez-carreras et al., 2010). Although
16
17 81 sediment fingerprinting studies of aeolian sands are not new (e.g. Pell et al., 1997;
18
19 82 Wasklewicz and Meek, 1995; Winspear and Pye, 1996; Liu et al., 2016; Muhs et al,
20
21 83 2017), challenges remain in adequately capturing the uncertainties associated with
22
23 84 the diverse sources and pathways that may exist, and adoption of techniques
24
25 85 developed in different disciplines offer a route forward. It is noteworthy that in a
26
27 86 recent review discussing applications of sediment source-tracing methods (Owens et
28
29 87 al., 2016), mention of aeolian sedimentation is limited to health science studies of
30
31 88 PM2.5 and PM10 material. The opportunity to utilize these approaches in aeolian
32
33 89 process science remains largely overlooked.
34
35
36
37
38
39
40
41
42
43
44
45
46
47
48
49
50
51
52
53
54
55
56
57
58
59
60

91 In recent years, increasing attention has been directed to the uncertainty of the
92 results generated by sediment source fingerprinting. It is important that such
93 uncertainty is recognized, particularly if the results are to be used to target
94 investment in sediment control measures (Mukundan et al., 2012). The factors
95 contributing to uncertainty in estimates of source apportionment are manifold and
96 diverse, and have been reviewed elsewhere (e.g. Walling 2010; Koiter et al., 2013;
97 Collins et al, 2017); here we consider some of the differences between the fluvial
98 setting of most sediment fingerprinting studies, and the aeolian context considered

1
2
3 99 here. Many uncertainties remain the same – for instance, instrumental precision.
4
5 100 Other aspects of the aeolian entrainment, transport and depositional system,
6
7 101 however, differ markedly from fluvial settings. Due to dominance of gravity in
8
9 102 controlling - and directing - slope and fluvial processes, and the (usually) confined
10
11 103 nature of fluvial systems, erosion and entrainment of sediment from catchments is
12
13 104 highly directionally-controlled. In an aeolian context, there is more scope for spatially
14
15 105 extensive direct entrainment of sediment, and also more potential for directional
16
17 106 variability, and this complex mixing environment may in turn lead to increased
18
19 107 covariance between properties used to derive the fingerprint. In addition, such
20
21 108 complexities cannot be considered static, as variations in wind regimes over long
22
23 109 timescales may lead to changes in these pathways.
24
25
26
27
28

29
30 111 In order to quantify the uncertainty associated to mixing models related to this
31
32 112 inherent variability in the source area and sediment mixture data, some recent
33
34 113 studies have explored the use of Monte Carlo simulations (e.g. Motha et al., 2003;
35
36 114 Collins et al., 2013; Collins et al., 2012; Stone et al., 2014; Smith & Blake, 2014;
37
38 115 Sherriff et al., 2015; Vale et al., 2016; Gellis & Noe, 2013; Voli et al., 2013; Wilkinson
39
40 116 et al., 2013; Walling et al., 2008). More recently, Bayesian mixing models being
41
42 117 employed more comprehensively translate component uncertainties into source
43
44 118 apportionment results (Cooper and Krueger, 2017) with several examples
45
46 119 undertaken in hydrological contexts (e.g. Fox & Papanicolaou, 2008; Cooper et
47
48 120 al., 2014; Cooper et al., 2015; Nosrati et al., 2014; Stewart et al., 2015). To date,
49
50 121 however, such approaches have not been used within aeolian sedimentary contexts.
51
52
53

54 122
55
56
57
58
59
60

1
2
3 123 The sophistication of aeolian sediment provenance studies currently lags those in
4
5 124 the fluvial sphere, and the main aim of this paper is to demonstrate the viability of
6
7 125 fingerprinting methods for aeolian sediments, including the estimation of uncertainty,
8
9 126 associated with the contributions from different geological units as potential sources
10
11 127 for a small dunefield, Ashkzar Erg, in the Yazd-Ardekan Plain, central Iran, using a
12
13 128 Bayesian mixing model. Ashkzar erg and its surrounding potential sources cause
14
15 129 many serious problems related to wind erosion and associated on-site and off-site
16
17 130 effects, with potential impacts on the health of the occupants of the neighbouring city
18
19 131 of Yazd (Naddafi et al., 2006). Aeolian deflation is a major erosional process on the
20
21 132 Yazd-Ardekan Plain and large amounts of aeolian sediment are often transported to
22
23 133 residential regions by wind (Amiraslani and Dragovich, 2011). Therefore, quantifying
24
25 134 sediment source contributions to the Ashkzar sand dunes could help to select the
26
27 135 best management strategies at this location and others similarly affected by aeolian
28
29 136 erosion. Additionally, the findings are considered in their geomorphological context
30
31 137 with the aim of explaining the spatial variability in sediment provenance observed at
32
33 138 Ashkzar erg.
34
35
36
37
38
39
40

139

140 **2. Materials and methods**

141 *2.1. Field location*

142 Yazd-Ardekan (31°10'–32°43' N, 53°68'–54°47' E) is an arid plain in central Iran,
143 and includes different geomorphic landscapes, such as the Ashkzar and Yazd ergs
144 (Figure 1). The Yazd-Ardekan Plain is surrounded by mountain ranges. These are
145 Shirkooch in the south, Ahangaran and the Margh Zard Mountains in the west, Haft
146 Adamin and Khoonzad Mountains in the east and Chak Chak Mountain in the north.
147 The area of the plain is ~2900 km², and it consists of 78% Quaternary alluvial fans

1
2
3 148 and terraces (Qt₂ geological unit), 13% clay flats (Qc geological unit), 7% Eocene
4
5 149 gypsiferous marl (Egm geological unit) and 2% sand dunes (Qsd geological unit)
6
7 150 (Figure 1 and 2). About 93% of Yazd-Ardekan Plain is thus covered by Quaternary
8
9 151 deposits. Active and stabilized sand dunes in the Ashkzar erg occupy 58 km²
10
11 152 (centred on 32° 1'N, 54° 10'E), which is dominated by barchans and transverse
12
13 153 barchanoid ridges (Figure 2). The erg has a sparse but extensive cover of *Haloxylon*
14
15 154 *persicum*, a species which is both endemic to the region, and is also used to stabilize
16
17 155 mobile sand (Amiraslani and Dragovich, 2011). Based on 50 years of climate data at
18
19 156 Yazd Meteorological Station, minimum and maximum annual temperatures are -16
20
21 157 °C and 46 °C, respectively. Long-term mean rainfall and annual evaporation in the
22
23 158 study area are ~60 mm/year and ~3500 mm/year respectively. According to annual
24
25 159 wind roses, dominant winds on the Yazd-Ardekan Plain are mainly from the north
26
27 160 and west (Figure 1C).
28
29
30
31
32
33

34 162 [Approx. location of Figure 1]
35
36 163

38 164 2.2. Sampling and laboratory analysis

40 165 The geological units that were identified as potential sources for sand dunes (Qsd
41
42 166 formation) are the Qt₂ (Quaternary alluvial fans and terraces), Qc (Quaternary clay
43
44 167 pans and flats) and Egm (Eocene marls) formations. Other surrounding lithologies in
45
46 168 the vicinity are hard, igneous exposures and can be discounted from generating
47
48 169 substantial quantities of deflatable sediment. In this study, spatially distributed
49
50 170 source samples were taken from 49 sites, covering the Egm (n=8), Qc (n=18) and
51
52 171 Qt₂ (n=23) potential sources, and eight sediment samples were collected from the
53
54 172 Ashkzar sand dunes (Figure 1D). Samples were collected from the upper 0–5 cm
55
56
57
58
59
60

1
2
3 173 depth of potential sources (that is, the layer of the regolith exposed to current aeolian
4
5 174 entrainment) and sand dunes (that is, the layer of the regolith most recently
6
7 175 deposited); this is similar to sampling strategies employed by other provenance
8
9 176 studies of aeolian dunes (e.g. Pell et al., 1997), and is accordance with common
10
11 177 earth science protocols (Owens et al., 2016). Within each source area, sample
12
13 178 selection was based upon locations that were: a) clearly derived from the geological
14
15 179 unit in question, b) selected to ensure broad spatial coverage of the source area, and
16
17 180 c) clearly influenced by aeolian erosion (e.g. the presence of deflatable unvegetated
18
19 181 sand surfaces with ripples, as well as yardangs of a range of scales). Samples
20
21 182 numbers were chosen to ensure a balance between the greater spatial extent of the
22
23 183 Qt2 unit (i.e. sampling was stratified), whilst maintaining a minimum of eight samples
24
25 184 for the smaller Egm and Qc units. The spatial location of sampling sites is shown in
26
27 185 Figure 1D.
28
29
30
31

32 186 All sand dune and potential source samples were dry sieved for particle size data,
33
34 187 and to isolate the 62.5-150 μm fraction for further geochemical analysis. This fraction
35
36 188 was chosen as it represents the dominant fraction in each of the dune samples
37
38 189 (Table 1), and is of a size range susceptible to aeolian transport (whilst excluding
39
40 190 any contribution of larger grains from local sources, either by aeolian creep or other
41
42 191 transport processes). Concentrations of elements including major, trace and rare
43
44 192 earth elements (REE) were determined using ICP-MS, after direct digestion with
45
46 193 aqua regia (e.g. Collins et al., 2010; Collins et al., 2012); and concentration of
47
48 194 strontium and neodymium isotopes measured by ICP-MS, after digestion with a
49
50 195 mixture of $\text{HNO}_3+\text{HClO}_4+\text{HF}$ (3:2:1) (e.g. Honda et al., 2004; Rao et al., 2011). The
51
52 196 relative standard deviation (%RSD), based on three replicates for each determinant
53
54 197 on each sample, was consistently $\leq 4\%$. With regards to REE concentrations, eight
55
56
57
58
59
60

1
2
3 198 REE ratios including Σ REE, Nd/Yb, Eu/Eu* (Europium Anomaly), (La/Lu)_n, (La/Sm)_n,
4
5 199 (Gd/Yb)_n, (La/Yb)_n and δ Ce (Cerium Anomaly) were calculated (e.g. Daga et al.,
6
7 200 2008; Dou et al., 2010; Rao et al., 2011). In total, 61 tracers were used to fingerprint
8
9 201 the sediments of the Yazd-Ardekan Plain.
10
11

12 202

13
14 203 [Approx. location of Table 1]
15

16 204 [Approx. location of Figure 2]
17

18 205 [Approx. location of Figure 3]
19

20 206

21 207 *2.3. Discrimination of aeolian sediment sources*

22
23
24
25 208 We employed a two-stage statistical method proposed by Collins and Walling (2007)
26
27 209 to characterize the composite fingerprint for the sources of the sands of the Ashkzar
28
29 210 dunes. In stage one, all individual fingerprint properties were tested for their ability to
30
31 211 distinguish source types, using the Kruskal–Wallis H-test. Properties with critical
32
33 212 values at the 95% level of confidence could be used in a composite fingerprinting
34
35 213 model to discriminate between sources types. In stage two, stepwise discriminant
36
37 214 function analysis (DFA) was employed to identify the optimum composite fingerprint
38
39 215 model from the properties selected in stage one. The stepwise DFA was based on
40
41 216 the minimization of Wilk's lambda was used to select optimum composite fingerprint.
42
43 217 The F values were used as the test criteria to enter and remove elements. The
44
45 218 threshold of F value for entering and removing of elements was set to 3.84 and 2.71,
46
47 219 respectively (e.g. Vale et al, 2016).
48
49

50 220 *2.4. Bayesian mixing model*

51
52
53
54
55
56
57
58
59
60

221 End-member mixing models have been taken a variety of approaches to account for
 222 uncertainty in the mixing model (Cooper and Krueger, 2017) and some (e.g. Brewer
 223 et al., 2005; Fox & Papanicolaou, 2008) have adopted hierarchical Bayesian models,
 224 which we adopt here. Within the mixing model formulation, we assume that, for each
 225 source s , the sample i tracer composition, x , has a multivariate normal distribution as
 226 follows:

$$227 \quad x_s^i \sim \text{MVN}_A(\mu_s, \Sigma_s), \quad s = 1, \dots, N, \quad i = 1, \dots, n_{x,s} \quad (\text{eq. 1})$$

228 where $n_{x,s}$ indicates the number of samples of source s ; μ_s is a A -dimensional vector
 229 representing mean fingerprints for source s ; Σ_s represents a $(A \times A)$ dimensional
 230 covariance matrix for source s . There are n_z sediment samples for which A
 231 fingerprints were measured for each sample $Z^j = (z_1^j, \dots, z_A^j)^T, j = 1, \dots, n_z$ and these
 232 fingerprints have multivariate normal distributions:

$$233 \quad Z^j \sim \text{MVN}_A(\mu_j^z, \Sigma^z) \quad (\text{eq. 2})$$

234 Each source s has a fractional contribution p_s^j to each sediment sample j . The
 235 contribution of source types for each sediment sample is equal to $p_s^j y_s^j$, where y_s^j is
 236 an unobserved (latent) variable that follow the same distribution as X_s^i .

$$237 \quad \mu_j^z = \sum_{s=1}^N p_s^j y_s^j, \quad j = 1, \dots, n_z \quad (\text{eq. 3})$$

$$238 \quad \sum_{s=1}^N p_s^j = 1, \quad 0 \leq p_s^j \leq 1 \quad (\text{eq. 4})$$

239 Each fractional contribution must be between zero and one, positive and all of them
 240 must sum to unity. To meet this constraint, some studies have used Dirichlet
 241 distribution as a prior for the fractional contribution (e.g. Fox & Papanicolaou, 2008;
 242 Massoudiehet al., 2013), whereas other studies used transformation such as

243 centered log-ratio (CLR) (Semmenset al., 2009), isometric log-ratio (ILR) (e.g.
 244 Cooper et al., 2015; Parnell et al., 2013; Egozcue et al., 2003) and additive log-ratio
 245 (ALR) (e.g. Brewer et al., 2005; Palmer & Douglas, 2008). In this study, a CLR
 246 transformation was used, as it has been shown to produce comparable median
 247 values to other methods, but with better precision (Cooper et al., 2014). The
 248 transformation applied is thus:

$$249 \quad \phi_i = CLR(P_i) = \log\left[\frac{P_{i1}}{g(P_i)}, \dots, \frac{P_{ik}}{g(P_i)}\right] \quad (\text{eq. 5})$$

$$250 \quad \phi_i \sim (\mu_\phi, \tau_\phi) \quad (\text{eq. 6})$$

251 where $g(p_i)$ is the geometric mean of the proportion vector. Figure 4 shows a
 252 directed acyclic graph of the model. Compared to an empirical Bayesian approach
 253 in which some prior parameters are estimated using deterministic data, the full
 254 Bayesian approach employed here needs to specify prior distribution for all
 255 parameters. When there is little information about the parameters, using informative
 256 hyper-parameters cause biased results. In this study, weakly or non-informative
 257 hyper-parameters were used. Multivariate normal and inverse-Wishart distributions
 258 were selected as prior distribution for sources means and covariance matrix,
 259 respectively.

$$260 \quad \mu_s^X \sim MVN(\theta_s, \tau_s^{-1}), \quad s = 1, \dots, N \quad (\text{eq.7})$$

$$261 \quad \Sigma_s^X \sim Inverse - Wishart(\Omega_s^X, \rho_s^X), \quad s = 1, \dots, N \quad (\text{eq.8})$$

262 Here, the hyper-parameter θ_s was set to the sample means of the fingerprints and
 263 τ_s was set as a diagonal matrix with values 0.01 on the diagonal. For Wishart
 264 distribution, the hyper-parameter Ω_s^X is a diagonal matrix with value 1 as diagonal

265 elements and ρ_S^X was set to six (to reflect the lack of information on the precision
 266 matrices, and the number of tracers selected for the fingerprint). Similar prior
 267 distribution and hyper-parameters was assigned for sediment covariance matrix.

$$268 \quad \Sigma^Z \sim \text{Inverse} - \text{Wishart}(\Omega, \rho) \quad (\text{eq.9})$$

269 Weakly informative hyper-parameters $N(0,1)$ and $\text{Inv-}\Gamma(2,1)$ were assigned for
 270 μ_ϕ and τ_ϕ , respectively.

271 The complete posterior distribution of all model parameters for sediment sample Z_j
 272 can thus be written as

$$273 \quad (\Sigma_S, \tau_\phi, \mu_\phi, \Sigma^Z, p_j, \phi, \mu_S | X, Z_j) \propto \prod_{S=1}^N \prod_{i=1}^{n_{x,s}} \{P(x_s^i | \mu_S, \Sigma_S)\} \times \prod_{S=1}^N P(\mu_S | \theta_S, \tau_S^{-1}) \times$$

$$274 \quad \prod_{S=1}^N P(\Sigma_S | \Omega_S, \rho_S) \times P(Z_j | \mu_j^Z, \Sigma^Z) \times P(\Sigma^Z | \Omega, \rho) \times P(\phi | \mu_\phi, \tau_\phi) \times P(\mu_\phi) \times P(\tau_\phi)$$

275 (eq.10)

276 As the joint posterior of all parameters is complex and high-dimensional, we cannot
 277 directly obtain posterior distribution functions, but the Bayesian model thus defined
 278 can be analyzed using Markov Chain Monte Carlo (MCMC); we have used the
 279 WinBUGS package (Lunn et al., 2000) to derive parameter estimates. MCMC
 280 methods require that the chain reaches a steady state, and the number of runs
 281 required to reach this state is considered as burn in. The model was run by taking
 282 50,000,000 times from the posterior distribution from the sand dune and source
 283 samples, and the first 5,000,000 runs were considered as burn in. The large number
 284 of iterations was used to ensure convergence, despite the model's complexity and
 285 high dimensionality; the model converged during the run, as assessed by trace plots
 286 of simulations, Monte Carlo error and autocorrelation.

287

1
2
3 288 [Approx. location of Figure 4]
4
5
6

7 289

8 290 **3. Results**

9
10 291 Grain size data are presented in Table 1 to enable consideration of potential sorting
11 292 effects during aeolian transportation. The sources reveal very similar physical grain
12 293 sizes, and it is worth noting that whilst the Qc unit is mapped as a 'clay flat', the
13 294 sediment sampled for analysis is dominantly sand. The erg, on the other hand, as
14 295 might be expected as a result of aeolian transport and deposition is better sorted,
15 296 and less enriched in the coarse and very coarse sand fraction. The individual dune
16 297 sand samples retain marked variability, with the very-fine (62.5-150 μm) fraction
17 298 ranging from 37% to 65%, and a single sample (8) retaining a substantial coarse (>
18 299 600 μm) component.
19
20
21
22
23
24
25
26
27
28
29

30 300

31
32 301 The Kruskal-Wallis H test (i.e. one-way ANOVA) was performed on geological units
33 302 Egm, Qc and Qt2. Results identified 25 significant tracers between these groups
34 303 (Table 2). Tracers that failed this test ($p > 0.05$) were removed. These were: Nd, Sm,
35 304 Gd, Tb, Dy, Yb, Lu, (Nd/Yb), (Gd/Yb)_n, (La/Sm)_n, V, Cr, Co, Ni, Cu, Zn, Y, Zr, Nb, Ta,
36 305 U, As, Bi, Cd, Ge, In, Mo, Sb, Se, Te, W, Mn, Si, ¹⁴³Nd, ¹⁴⁴Nd and ⁸⁶Sr. Whilst the
37 306 successful discrimination of different tracers between geological units will vary when
38 307 this method is applied to settings other than this location, the presence of 25 tracers
39 308 with significant discriminatory power suggests that this method may be applicable in
40 309 diverse geological settings and/or areas with contrasting weathering regimes.
41
42
43
44
45
46
47
48
49
50

51 310

52
53
54 311 [Approx. location of Table 2]
55

56 312
57
58
59
60

1
2
3 313 According to the DFA, a total of six individual tracer properties (Rb, Sr, ⁸⁷Sr,
4
5 314 (La/Yb)_n, Ga and δCe) were selected for the optimum composite fingerprint, which
6
7 315 correctly discriminated 81.6% of the source type samples (Figure 5).
8
9

10 316

11 317 [Approx. location of Table 3]

12
13 318 [Approx. location of Figure 5]
14
15

16 319

17 320 Although DFA results suggested that good source discrimination was achieved, with
18
19 321 clear separation of the three group centroids, samples sourced from Qc were found
20
21 322 to slightly overlap with the Qt2 source when the first two discriminant functions were
22
23 323 plotted, and, to a lesser degree Qt2 and Egm also overlap slightly (Figure 5). The
24
25 324 mean and SD of six optimum composite fingerprints that were selected for the
26
27 325 Bayesian mixing model, are presented in Table 3. These were tested for normality
28
29 326 via Wilks-Shapiro tests (Table 4), and the raw data revealed that the Sr and δCe
30
31 327 tracers did not follow a normal distribution for all settings. To account for this, Box-
32
33 328 Cox transformations (Box and Cox, 1964) were applied to all data, and the
34
35 329 transformed data were used for model experimentation.
36
37
38
39

40 330

41 331 [Approx. location of Table 4]
42
43

44 332

45
46 333 The derived source contributions for the eight sand dune samples are presented in
47
48 334 Table 5 and Figure 6. Overall, the alluvial fans and terraces (Qt2) provide the most
49
50 335 abundant supply of sands (mean contribution across all 8 samples = 45.4%, and
51
52 336 locally up to 92.7%), with the clay pans (Qc) and Eocene marls (Egm) each
53
54 337 contributing around a quarter of the net sediment aeolian flux. However, the
55
56 338 composition of the dune sands is highly variable, with different samples dominated
57
58
59
60

1
2
3 339 by different contributing sources, and locally, all three of the potential sources occur
4
5 340 as both maxima and minima.
6

7 341

8
9 342 [Approx. location of Figure 6]
10

11
12 343

13 14 344 **4. Discussion**

15 16 17 345 4.1 Development of a Bayesian mixing model to discriminate aeolian sediment 18 19 346 pathways

20
21
22
23 347 The mixing model to fingerprint aeolian sediment sources deployed in this study
24
25 348 used composite signature comprising a suite of six geochemical characteristics (Rb,
26
27 349 Sr, ^{87}Sr , La:Yb, Ga and δCe) identified by stepwise DFA as the most appropriate,
28
29 350 and was able to account for >82% of the variance between the three sources. The
30
31 351 suite of properties selected by the DFA method most likely reflects two principal
32
33 352 factors; the ultimate source of the sediments, and the degree of weathering. The
34
35 353 latter might well have variable influence across the source areas, and hence there is
36
37 354 some overlap between samples of each class. High La:Yb ratios, for instance, are
38
39 355 typically associated with deep igneous lithogenesis (Deffant and Drummond, 1990)
40
41 356 and may locally reflect differing sediment contributions from the Precambrian
42
43 357 crystalline basement provinces of central Iran. δCe , similarly, is often associated with
44
45 358 intrusive igneous rocks, although may also be enriched in some sedimentary rocks
46
47 359 (Wedepohl, 1978); in this study, the highest concentrations are found in the alluvial
48
49 360 fans derived from the adjacent igneous mountains, but the second highest
50
51 361 concentrations are found in the sedimentary marls of the Egm unit (Figure 2). In
52
53 362 short, the highly varied geology of central Iran, ranging from Precambrian magmatic
54
55
56
57
58
59
60

1
2
3 363 rocks to Cenozoic marine sediments, promotes a high degree of variance in the
4
5 364 geochemical fingerprint of modern aeolian sediments. Compounding this is the range
6
7 365 of weathering intensities seen, from the intense weathering history of the sediments
8
9
10 366 of Quaternary clay pans, to the more moderate weathering of the sands of the
11
12 367 alluvial fans forming the piedmonts of the neighbouring ranges.

13
14
15 368 4.2 Potential for application to other aeolian depositional settings

16
17
18 369 Despite the usefulness of understanding the provenance of aeolian sands, the
19
20 370 sophistication of unmixing models within the aeolian science community generally
21
22 371 lags that of fluvial science, in particular in terms of the numerical underpinning of
23
24 372 methods applied. Indeed, many such studies attempt to derive provenance estimates
25
26 373 only qualitatively (e.g. Fitzsimmons et al, 2009), or, in the few recent cases where
27
28 374 robust unmixing models have been applied, relatively simple approaches to
29
30 375 incorporating uncertainty into models have been taken (e.g. Liu et al., 2016).

31
32
33
34 376 The successful application of a Bayesian model within an MCMC framework to
35
36 377 aeolian sands of a small erg in this study demonstrates the potential of this approach
37
38 378 more widely. It is particularly likely to complement detrital zircon U-Pb dating
39
40 379 provenance studies, and may prove especially useful in settings where there are
41
42 380 insufficient zircon grains to enable the application of this method (e.g. Jia et al.,
43
44 381 2015, Nie and Peng, 2014, Ren et al., 2014, Thorpe et al., 1992). Further application
45
46 382 of the methods demonstrated here is required to test the ability of such methods
47
48 383 globally, but these results suggest a promising future, and a new direction for aeolian
49
50 384 provenance studies. For instance, it would be useful to explore the power of these
51
52 385 methods in larger-scale settings, such as the continental dunefields of southern
53
54 386 Africa and Australia, where provenance studies have been used to explore the
55
56
57
58
59
60

1
2
3 387 relationship between tectonic setting and sedimentation (e.g. Garzanti et al., 2014)
4
5 388 and explore the long-term evolution of landscapes (e.g. Pell et al., 1997; 2000). This
6
7 389 will also elucidate the importance of diversity of local geology and weathering
8
9 390 regimes in producing sufficiently distinctive fingerprints.

11
12 391 Accurate propagation of the uncertainties associated with the component
13
14 392 contributions is also a valuable aspect of the methodology employed here and allows
15
16 393 more realistic interpretation of the data. For instance, the most abundant two source
17
18 394 components of samples E (Qt2 = 62.3%; Qc = 23%) and D (Egm = 56.3%; Qc =
19
20 395 28.7%) might suggest similar proportions of the major components at these dunes;
21
22 396 roughly 60:25. However, consideration of the lower confidence of the fingerprint of
23
24 397 sample D (Figure 6) reveals that whilst the composition of this sample is much more
25
26 398 open to interpretation, sample E is quite clearly dominated by the alluvial fan-derived
27
28 399 sands (Qt2).

30
31
32
33
34 400

35 36 401 4.3 Implications for aeolian sediment transport pathways

37
38
39 402 Overall, the surrounding Quaternary fans and terraces contribute most (~45%) to the
40
41 403 composition of Ashkzar erg; yet this is a disproportionately low value, given that they
42
43 404 represent 78% of the surrounding area. Conversely, the size of the overall
44
45 405 contributions from the Quaternary clay flats (~26%) and Eocene marls (~28%) to the
46
47 406 samples studied reveals the importance of these landscape units as sediment
48
49 407 sources, given that these units occupy only 13% and 7% of the surrounding area,
50
51 408 respectively. The importance of the marls as a source sediment, which outcrop only
52
53 409 to the north of the Ashkzar dunefield, suggests that net wind regime alone cannot be
54
55 410 considered as indicative of the net sediment transport in the region (Figure 1), as
56
57
58
59
60

1
2
3 411 westerly winds are equally strong here yet import much less sediment. Both the wind
4
5 412 regime and potential sediment sources must be considered when evaluating net
6
7 413 aeolian sediment flux.
8
9

10 414 There is much spatial variation in the composition of the dune sands of Ashkzar erg
11
12 415 (Figure 6). Even before the geochemical composition of these sands is considered,
13
14 416 such variability is evident from the differing grain size profiles in the eight samples
15
16 417 investigated here (Table 1). Sample G, from the far south of the dunefield, contains
17
18 418 ~20% coarse sands (defined here as $> 600 \mu\text{m}$), an unusually high figure for an
19
20 419 aeolian dune, although this sample is taken close to the border with the mapped
21
22 420 region of slipfaceless dome dunes, which tend to accumulate from coarser sands
23
24 421 (Lancaster, 1995). That said, sample H, from within the dome dunes, is not unusually
25
26 422 coarse.
27
28
29

30
31 423 Broadly, and considering the uncertainties presented by the methodology proposed
32
33 424 herein, two groups can be discerned within the samples geochemically analysed for
34
35 425 provenance (Figure 6). Samples taken from along the south and west of the
36
37 426 dunefield (B, E, F and G) are dominated to varying degrees by sediment from the
38
39 427 surrounding Quaternary fans and terraces (i.e. source unit Qt2), whereas most
40
41 428 samples to the north and east (A, D and H) show much greater contributions from
42
43 429 the Eocene marls (Egm) and clay flats (Qc). However, the division is not clear-cut;
44
45 430 sample C, in the northeast of the dunefield, has a dominant component from the Qt2
46
47 431 unit (with the second component only very slightly overlapped at 2σ confidence
48
49 432 levels). It is, perhaps, unsurprising that the more northerly samples tend to show an
50
51 433 increased input from the Eocene marls (Egm), as these units have been shown to
52
53 434 contribute disproportionately to the sediment flux in the area, and also outcrop
54
55 435 exclusively on the northern side of the valley (Figure 1).
56
57
58
59
60

1
2
3 436 The provenance of the sands is even less readily correlated with dune morphology,
4
5 437 with the Qt₂-dominated sands occurring within three defined dune morphological
6
7 438 zones (barchans, barchanoid ridges and asymmetrical barchans). Samples A and B,
8
9 439 the closest pair of samples studied (~2.2 km apart), yield very different provenance
10
11 440 fingerprints, despite both lying within the region of Ashkzar erg dominated by
12
13 441 barchanoid ridges. The overall morphology of the dunes (Figure 3) supports spatially
14
15 442 and /or temporally variable sediment availability, with the transformation of barchans
16
17 443 to barchanoid ridges essentially being sediment-supply controlled, and asymmetric
18
19 444 barchan/linear forms believed to be the result of asymmetries of sediment supply, or
20
21 445 changes to the wind regime (Bagnold, 1941; Lancaster 1995).
22
23
24
25

26 446 The heterogeneity in the sediment provenance evident here suggests that either a)
27
28 447 some kind of fractionation of the aeolian sediment flux is occurring, with different
29
30 448 sources depositing sediment at different locations or b) different sediment transport
31
32 449 pathways have been active intermittently and asynchronously during the formation of
33
34 450 the dunefield. The similar physical composition (i.e. grain size) of the sources, and
35
36 451 the lack of evidence of systematic variation across the dunefield, would tend to
37
38 452 support the latter suggestion. Different sediment pathways might result from different
39
40 453 sources become more or less active over time, or might result from changing wind
41
42 454 regime over long (i.e. late Quaternary) timescales. The heterogeneity evident also
43
44 455 suggests that during dune accumulation periods, large-scale mixing of aeolian sands
45
46 456 from different sources (which might be expected given transport distances of 10-50
47
48 457 km) is not occurring. In the absence of any chronological control for these dunes,
49
50 458 such hypotheses cannot be conclusively tested currently, but establishing the
51
52 459 relative roles of spatial and temporal variability in dune accumulation would be a
53
54 460 worthwhile exercise.
55
56
57
58
59
60

1
2
3 461
4
56 462 **5. Conclusion**
7

8
9 463 In dryland environments, understanding the main sources for aeolian sediments is
10
11 464 an essential step in developing management strategies to reduce aeolian sediment
12
13 465 loadings and wind erosion. Establishing aeolian sediment pathways, however, is not
14
15 466 usually straightforward and is complicated when multiple potential source areas
16
17 467 might contribute to a region of net sand accumulation. The method proposed here,
18
19 468 based on methodologies applied to fluvial sediments, uses a suite of geochemical
20
21 469 data to identify the most apposite characteristics (the 'fingerprint') for discerning
22
23 470 superficially similar sources of aeolian sediment. Whereas these methods have
24
25 471 become widely adopted in fluvial geomorphology and catchment science over the
26
27 472 past two decades, they remain almost unused in aeolian science. Here, it has been
28
29 473 successfully demonstrated on fine sand in a small dunefield in central Iran, but it
30
31 474 might be applied equally to dust (i.e. silt) flux, although longer transport distances are
32
33 475 liable to prove more difficult to fingerprint unless relatively discrete and distinct
34
35 476 sources can be identified. The use of MCMC methods to provide confidence
36
37 477 estimates in the mixing model output enables more rigorous interpretation of the
38
39 478 relative importance of different sediment sources.
40
41
42
43
44

45 479

46
47 480 This method revealed within Ashkzar erg unexpected spatial heterogeneity of dune
48
49 481 composition (and thus provenance), which has a complex relationship with the
50
51 482 position within the dunefield, the dune type and other physical characteristics. The
52
53 483 Eocene marls in the surrounding area have been shown to contribute
54
55 484 disproportionately to the sediments of the dunes. In terms of management of sand
56
57 485 and dust hazard at this location, both the original source areas and those parts of the
58
59
60

1
2
3 486 dunefield enriched in the Egm component might be viewed as priority targets for
4
5 487 landscape stabilization efforts, due to their apparent propensity for aeolian
6
7 488 mobilization.
8

9
10 489

11
12 490 More widely, the methods proposed here for aeolian provenance unmixing method
13
14 491 can be applied to any mixed-source aeolian sediment to elucidate differing
15
16 492 susceptibilities to aeolian deflation, and reveal transport pathways at timescales
17
18 493 longer than those possible by either field study or remote sensing. Disciplines which
19
20 494 might benefit from the adoption of such methods include not just aeolian
21
22 495 geomorphology, but also dryland land management, soil science, engineering
23
24 496 geology and potentially palaeoenvironmental and palaeoclimatological studies. A
25
26 497 combination of the methods presented herein with geochronological studies may
27
28 498 enable calculation of flux rates to provide quantification of long-term sediment fluxes,
29
30 499 even when, as is very often the case with aeolian sediments, transport pathways are
31
32 500 complex and multi-phase.
33
34
35

36 501

37
38 502

39 40 503 **References**

41
42
43 504 Amiraslani, F. and Dragovich, D. (2011). Combating desertification in Iran over the
44
45 505 last 50 years: An overview of changing approaches. *Journal of Environmental*
46
47 506 *Management* 92 (1), 1-13. doi: 10.1016/j.jenvman.2010.08.012.
48
49

50
51 507 Bagnold, R.A. 1941. The physics of blown sand. Methuen, London.
52

53
54 508 Box, G.E.P & Cox, D.R. (1964). An analysis of transformations. *Journal of the Royal*
55
56 509 *Statistical Society, Series B.* 26 (2): 211–252.
57
58
59
60

- 1
2
3 510 Brewer, M. J., Filipe, J. A. N., Elston, D. A., Dawson, L. A., Mayes, R. W., Soulsby,
4
5 511 Ch., & Dunn, S. M. (2005). A Hierarchical Model for Compositional Data
6
7 512 Analysis. *Journal of Agricultural, Biological, and Environmental Statistics*, 10(1),
8
9 513 19–34. doi:10.1198/108571105X28200
- 11
12 514 Chen, F., Fang, N., & Shi, Z. (2016). Using biomarkers as fingerprint properties to
13
14 515 identify sediment sources in a small catchment. *Science of the Total*
15
16 516 *Environment*, 557-558, 123–133. doi:10.1016/j.scitotenv.2016.03.028
- 17
18
19
20 517 Collins, A. L., & Walling, D. E. (2007). Sources of fine sediment recovered from the
21
22 518 channel bed of lowland groundwater-fed catchments in the UK. *Geomorphology*,
23
24 519 88, 120–138. doi:10.1016/j.geomorph.2006.10.018
- 25
26
27
28 520 Collins, A. L., Zhang, Y., McChesney, D., Walling, D. E., Haley, S. M., & Smith, P.
29
30 521 (2012). Sediment source tracing in a lowland agricultural catchment in southern
31
32 522 England using a modified procedure combining statistical analysis and
33
34 523 numerical modelling. *Science of the Total Environment*, 414, 301–317.
35
36 524 doi:10.1016/j.scitotenv.2011.10.062
- 37
38
39 525 Collins, A. L., Zhang, Y. S., Duethmann, D., Walling, D. E., & Black, K. S. (2013).
40
41 526 Using a novel tracing-tracking framework to source fine-grained sediment loss to
42
43 527 watercourses at sub-catchment scale. *Hydrological Processes*, 27(6), 959–974.
44
45 528 doi:10.1002/hyp.9652
- 46
47
48
49 529 Collins, A. L., Zhang, Y., Walling, D. E., Grenfell, S. E., & Smith, P. (2010). Tracing
50
51 530 sediment loss from eroding farm tracks using a geochemical fingerprinting
52
53 531 procedure combining local and genetic algorithm optimisation. *Science of the*
54
55 532 *Total Environment*, 408(22), 5461–5471. doi:10.1016/j.scitotenv.2010.07.066

- 1
2
3 533 Collins, A. L., Zhang, Y., Walling, D. E., Grenfell, S. E., Smith, P., Grischeff, J., ...
4
5 534 Brogden, D. (2012). Quantifying fine-grained sediment sources in the River Axe
6
7 535 catchment, southwest England: Application of a Monte Carlo numerical
8
9 536 modelling framework incorporating local and genetic algorithm optimisation.
10
11 537 *Hydrological Processes*, 26(13), 1962–1983. doi:10.1002/hyp.8283
12
13
14
15 538 Collins, A.L., Pulley, S., Foster, I.D.L., Gellis A., Porto, P., Horowitz, A.J. (2016).
16
17 539 Sediment source fingerprinting as an aid to catchment management: A review of
18
19 540 the current state of knowledge and a methodological decision-tree for end-
20
21 541 users. *Journal of Environmental Management*, 194, 86–108.
22
23 542 doi.org/10.1016/j.jenvman.2016.09.075
24
25
26
27 543 Cooper RJ and Krueger T (2017, in press). An extended Bayesian sediment
28
29 544 fingerprinting mixing model for the full Bayes treatment of geochemical
30
31 545 uncertainties. *Hydrological Processes*. DOI: 10.1002/hyp.11154.
32
33
34 546 Cooper, R. J., Krueger, T., Hiscock, K. M., & Rawlins, B. G. (2014). Sensitivity of
35
36 547 fluvial sediment source apportionment to mixing model assumptions: A
37
38 548 Bayesian model comparison. *Water Resources Research*, 9031–9047.
39
40 549 doi:10.1002/2014WR016194.
41
42
43
44 550 Cooper, R. J., Krueger, T., Hiscock, K. M., & Rawlins, B. G. (2015). High-temporal
45
46 551 resolution fluvial sediment source fingerprinting with uncertainty: A Bayesian
47
48 552 approach. *Earth Surface Processes and Landforms*, 40(1), 78–92.
49
50 553 doi:10.1002/esp.3621
51
52
53
54 554 Daga, R., Ribeiro Guevara, S., Sánchez, M. L., & Arribére, M. (2008). Source
55
56 555 identification of volcanic ashes by geochemical analysis of well preserved
57
58
59
60

- 1
2
3 556 lacustrine tephra in Nahuel Huapi National Park. *Applied Radiation and*
4
5 557 *Isotopes*, 66(10), 1325–1336. doi:10.1016/j.apradiso.2008.03.009
6
7
8 558 Defant, M.J. and Drummond, M.S. 1990. Derivation of some modern arc magmas by
9
10 559 melting of young subducted lithosphere. *Nature* 367, 662–665
11
12
13 560 Delmonte, B., Baroni, C., Andersson, P.S., Schoberg, H., Hansson, M., Aciego, S.,
14
15 561 Petit, J.-R., Albani, S., Mazzola, C., Maggi, V., Frezzotti, M., 2010. Aeolian dust
16
17 562 in the Talos Dome ice core (East Antarctica, Pacific/Ross Sea sector): Victoria
18
19 563 Land versus remote sources over the last two climate cycles. *Journal of*
20
21 564 *Quaternary Science* 25, 1327-1337.
22
23
24
25 565 Delmonte, B., Basile-Doelsch, I., Petit, J.R., Maggi, V., Revel-Rolland, M., Michard,
26
27 566 A., Jagoutz, E., Grousset, F., 2004. Comparing the Epica and Vostok dust
28
29 567 records during the last 220,000 years: stratigraphical correlation and
30
31 568 provenance in glacial periods. *Earth-Science Reviews* 66, 63-87.
32
33
34
35 569 Dou, Y., Yang, S., Liu, Z., Clift, P. D., Shi, X., Yu, H., & Berne, S. (2010).
36
37 570 Provenance discrimination of siliciclastic sediments in the middle Okinawa
38
39 571 Trough since 30ka: Constraints from rare earth element compositions. *Marine*
40
41 572 *Geology*, 275(1-4), 212–220. doi:10.1016/j.margeo.2010.06.002
42
43
44
45 573 Douglas, G., Caitcheon, G., & Palmer, M. (2009). Sediment source identification and
46
47 574 residence times in the Maroochy River estuary, southeast Queensland,
48
49 575 Australia. *Environmental Geology*, 57(3), 629–639. doi:10.1007/s00254-008-
50
51 576 1336-7
52
53
54 577 Egozcue, J. J., Pawlowsky-Glahn, V., Mateu-Figueras, G., & Barceló-Vidal, C.
55
56 578 (2003). Isometric Logratio Transformations for Compositional Data Analysis.
57
58
59
60

- 1
2
3 579 *Mathematical Geology*, 35(3), 279–300. doi:10.1023/A:1023818214614
4
5
6 580 Fox, J. F., & Papanicolaou, A. N. (2008). An un-mixing model to study watershed
7
8 581 erosion processes. *Advances in Water Resources*, 31, 96–108.
9
10 582 doi:10.1016/j.advwatres.2007.06.008
11
12
13 583 Garzanti, E., Vermeesch, P., Ando, S., Vezzoli, G., Valagussa, M., Allen, K., Kadi,
14
15 584 K.A., Al-Juboury, A.I.A., 2013. Provenance and recycling of Arabian desert
16
17 585 sand. *Earth-Science Reviews*. 120, 1-19.
18
19
20
21 586 Garzanti, E., Vermeesch, P., Padoan, M., Resentini, A., Vezzoli, G., Ando, S., 2014.
22
23 587 Provenance of Passive-Margin Sand (Southern Africa). *Journal of Geology*,
24
25 588 122(1), 17-42. doi:10.1086/674803
26
27
28 589 Gellis, A. C., & Noe, G. B. (2013). Sediment source analysis in the Linganore Creek
29
30 590 watershed, Maryland, USA, using the sediment fingerprinting approach: 2008 to
31
32 591 2010. *Journal of Soils and Sediments*, 13(10), 1735–1753. doi:10.1007/s11368-
33
34 592 013-0771-6
35
36
37
38 593 Haddadchi, A, Ryder, D.S., Evrard, O., Olley, J. (2013). Sediment fingerprinting in
39
40 594 fluvial systems: review of tracers, sediment sources and mixing models. *Int. J.*
41
42 595 *Sediment Res.*, 28, 560–578
43
44
45 596 Huntsman-Mapila, P., Kampunzu, A.B., Vink, B., Ringrose, S., 2005. Cryptic
46
47 597 indicators of provenance from the geochemistry of the Okavango Delta
48
49 598 sediments, Botswana. *Sedimentary Geology* 174, 123-148.
50
51
52
53 599 Honda, M., Yabuki, S., & Shimizu, H. S. H. I. (2004). Geochemical and isotopic
54
55 600 studies of aeolian sediments in China. *Sedimentology*, 211–230.
56
57 601 doi:10.1046/j.1365-3091.2003.00618.x
58
59
60

- 1
2
3 602 Jia, Y., Fu, B., Jolivet, M. and Zheng, S. Cenozoic tectono-geomorphological growth
4
5 603 of the SW Chinese Tian Shan: insight from AFT and detrital zircon U-Pb data.
6
7 604 *Journal of Asian Earth Sciences*, 2015, 111, 395-413.
8
9
10 605 Koiter, A. J., Owens, P. N., Petticrew, E. L., & Lobb, D. A. (2013). The behavioural
11
12 606 characteristics of sediment properties and their implications for sediment
13
14 607 fingerprinting as an approach for identifying sediment sources in river basins.
15
16 608 *Earth-Science Reviews*, 125, 24–42. doi:10.1016/j.earscirev.2013.05.009
17
18
19
20 609 Lancaster, N. 1995. *Geomorphology of Desert Dunes*. Routledge, London.
21
22
23 610 Lin, J., Huang, Y., Wang, M. kuang, Jiang, F., Zhang, X., & Ge, H. (2015). Assessing
24
25 611 the sources of sediment transported in gully systems using a fingerprinting
26
27 612 approach: An example from South-east China. *Catena*, 129, 9–17.
28
29 613 doi:10.1016/j.catena.2015.02.012
30
31
32
33 614 Liu, B.L., Niu, Q.H., Qu, J.J., Zu, R.P. (2016). Quantifying the provenance of aeolian
34
35 615 sediments using multiple composite fingerprints. *Aeolian Research*, 22, 117-
36
37 616 122. doi:10.1016/j.aeolia.2016.08.002
38
39
40 617 Lunn, D.J., Thomas, A., Best, N., and Spiegelhalter, D. (2000) WinBUGS -- a
41
42 618 Bayesian modelling framework: concepts, structure, and extensibility. *Statistics*
43
44 619 *and Computing*, 10:325--337.
45
46
47
48 620 Martínez-Carreras, N., Udelhoven, T., Krein, A., Gallart, F., Iffly, J. F., Ziebel, J. and
49
50 621 Walling, D. E. (2010). The use of sediment colour measured by diffuse
51
52 622 reflectance spectrometry to determine sediment sources: Application to the
53
54 623 Attert River catchment. *Journal of Hydrology*, 382(1-4), 49–63.
55
56 624 doi:10.1016/j.jhydrol.2009.12.017
57
58
59
60

- 1
2
3 625 Massoudieh, A., Gellis, A., Banks, W. S., & Wieczorek, M. E. (2013). Suspended
4
5 626 sediment source apportionment in Chesapeake Bay watershed using Bayesian
6
7 627 chemical mass balance receptor modeling. *Hydrological Processes*, 27(24),
8
9 628 3363–3374. doi:10.1002/hyp.9429
- 11
12 629 Motha, J. A., Wallbrink, P. J., Hairsine, P. B., & Grayson, R. B. (2003). Determining
13
14 630 the sources of suspended sediment in a forested catchment in southeastern
15
16 631 Australia. *Water Resources Research*, 39(3), 1056. doi:10.1029/2001wr000794
- 17
18
19
20 632 Muhs, D. R., Lancaster, N. and Skipp, G.L. (2017). A complex origin for the Kelso
21
22 633 Dunes, Mojave National Preserve, California, USA: A case study using a simple
23
24 634 geochemical method with global applications. *Geomorphology*, 276, 222-243.
25
26 635 doi: 10.1016/j.geomorph.2016.10.002
- 27
28
29
30 636 Mukundan, R., Walling, D. E., Gellis, A. C., Slattery, M. C., & Radcliffe, D. E. (2012).
31
32 637 Sediment Source Fingerprinting: Transforming From a Research Tool to a
33
34 638 Management Tool. *Journal of the American Water Resources Association*,
35
36 639 48(6), 1241–1257. doi:10.1111/j.1752-1688.2012.00685.x
- 37
38
39 640 Naddafi, K., Nabizadeh, R., Soltanianzadeh, Z., Ehrampoosh, M.H., 2006.
40
41 641 Evaluation of dustfall in the air of Yazd. *Journal of Environmental Health*
42
43 642 *Science and Engineering*, 3, 161-168.
- 44
45
46
47 643 Nanson, G.C., Chen, X.Y., Price, D.M. (1995). Aeolian and fluvial evidence of
48
49 644 changing climate and wind patterns during the past 100 Ka in the Western
50
51 645 Simpson Desert, Australia. *Palaeogeography Palaeoclimatology Palaeoecology*
52
53 646 113, 87-102.
- 54
55
56
57 647 Nie, J. and Peng, W. (2014). Automated SEM–EDS heavy mineral analysis reveals
58
59
60

- 1
2
3 648 no provenance shift between glacial loess and interglacial paleosol on the
4
5 649 Chinese Loess Plateau. *Aeolian Research* 13, 71-75.
6
7
8 650 Nosrati, K., Govers, G., Semmens, B. X., & Ward, E. J. (2014). A mixing model to
9
10 651 incorporate uncertainty in sediment fingerprinting. *Geoderma* 217-218, 173–180.
11
12 652 doi:10.1016/j.geoderma.2013.12.002
13
14
15 653 Owens, P.N., Blake, W.H., Gaspar, L., Gateuille, D., Koiter, A.J., Lobb, D.A.,
16
17 654 Petticrew, E.L., Reiffarth, D.G., Smith, H.G. & Woodward, J.C. (2016).
18
19 655 Fingerprinting and tracing the sources of soils and sediments: Earth and ocean
20
21 656 science, geoarchaeological, forensic, and human health applications. *Earth-*
22
23 657 *Science Reviews*, 162, 1-23. doi: 10.1016/j.earscirev.2016.08.012
24
25
26
27 658 Palmer, M. J., & Douglas, G. B. (2008). A Bayesian statistical model for end member
28
29 659 analysis of sediment geochemistry, incorporating spatial dependences. *Journal*
30
31 660 *of the Royal Statistical Society. Series C: Applied Statistics* 57(3), 313–327.
32
33 661 doi:10.1111/j.1467-9876.2007.00615.x
34
35
36
37 662 Parnell, A. C., Phillips, D. L., Bearhop, S., Semmens, B. X., Ward, E. J., Moore, J.
38
39 663 W., Inger, R. (2013). Bayesian stable isotope mixing models. *Environmetrics*
40
41 664 24(6), 387–399. doi:10.1002/env.2221
42
43
44
45 665 Pell, S.D., Williams, I.S., Chivas, A.R., 1997. The use of protolith zircon-age
46
47 666 fingerprints in determining the protosource areas for some Australian dune
48
49 667 sands. *Sedimentary Geology* 109, 233-260.
50
51
52 668 Pell, S.D., Chivas, A.R., Williams, I.S. 2000. The Simpson, Strzelecki and Tirari
53
54 669 Deserts: development and sand provenance. *Sedimentary Geology* 130 (1-2),
55
56 670 107–130. doi: 10.1016/S0037-0738(99)00108-6
57
58
59
60

- 1
2
3 671 Pethierick, L., McGowan, H., Moss, P., 2008. Climate variability during the Last
4
5 672 Glacial Maximum in eastern Australia: evidence of two stadials? *Journal of*
6
7 673 *Quaternary Science* 23, 787-802.
- 8
9
10 674 Pittam, N. J., Foster, I. D. L., & Mighall, T. M. (2009). An integrated lake-catchment
11
12 675 approach for determining sediment source changes at Aqualate Mere, Central
13
14 676 England. *Journal of Paleolimnology*, 42(2), 215–232. doi:10.1007/s10933-008-
15
16 677 9272-9
- 17
18
19
20 678 Rao, W., Tan, H., Jiang, S., & Chen, J. (2011). Trace element and REE
21
22 679 geochemistry of fine- and coarse-grained sands in the Ordos deserts and links
23
24 680 with sediments in surrounding areas. *Chemie Der Erde - Geochemistry*, 71(2),
25
26 681 155–170. doi:10.1016/j.chemer.2011.02.003
- 27
28
29
30 682 Ren, R., Han, B-F., Xu, Z. and Li, Q. 2014. When did the subduction first initiate in
31
32 683 the southern Paleo-Asian Ocean: New constraints from a Cambrian intra-
33
34 684 oceanic arc system in West Junggar, NW China. *Earth and Planetary Science*
35
36 685 *Letters* 388, 222–236
- 37
38
39 686 Semmens, B. X., Moore, J. W., & Ward, E. J. (2009). Improving Bayesian isotope
40
41 687 mixing models: A response to Jackson et al. (2009). *Ecology Letters*, 12(3), 10–
42
43 688 12. doi:10.1111/j.1461-0248.2009.01283.x
- 44
45
46
47 689 Sherriff, S. C., Franks, S. W., Rowan, J. S., Fenton, O., & Ó'hUallacháin, D. (2015).
48
49 690 Uncertainty-based assessment of tracer selection, tracer non-conservativeness
50
51 691 and multiple solutions in sediment fingerprinting using synthetic and field data.
52
53 692 *Journal of Soils and Sediments*, 15(10), 2101–2116. doi:10.1007/s11368-015-
54
55 693 1123-5

- 1
2
3 694 Smith, H. G., & Blake, W. H. (2014). Sediment fingerprinting in agricultural
4
5 695 catchments: A critical re-examination of source discrimination and data
6
7 696 corrections. *Geomorphology*, 204, 177–191.
8
9
10 697 doi:10.1016/j.geomorph.2013.08.003
11
12
13 698 Stewart, H. A., Massoudieh, A., & Gellis, A. (2015). Sediment source apportionment
14
15 699 in Laurel Hill Creek, PA, using Bayesian chemical mass balance and isotope
16
17 700 fingerprinting. *Hydrological Processes*, 29(11), 2545–2560.
18
19 701 doi:10.1002/hyp.10364
20
21
22 702 Stone, M., Collins, A. L., Silins, U., Emelko, M. B., & Zhang, Y. S. (2014). The use of
23
24 703 composite fingerprints to quantify sediment sources in a wildfire impacted
25
26 704 landscape, Alberta, Canada. *Science of the Total Environment*, 473-474, 642–
27
28 705 650. doi:10.1016/j.scitotenv.2013.12.052
29
30
31
32 706 Thorpe, R.I., Hickman, A.H., Davis, D.W., Mortensen, J.K. and Trendall, A.F., 1992.
33
34 707 U/Pb zircon geochronology of Archaean felsic units in the Marble Bar region,
35
36 708 Pilbara Craton, Western Australia. *Precambrian Research*, 56, 169-189.
37
38
39 709 Vale, S. S., Fuller, I. C., Procter, J. N., Basher, L. R., & Smith, I. E. (2016).
40
41 710 Characterization and quantification of suspended sediment sources to the
42
43 711 Manawatu River, New Zealand. *Science of The Total Environment*, 543, 171–
44
45 712 186. doi:10.1016/j.scitotenv.2015.11.003
46
47
48
49 713 Voli, M. T., Wegmann, K. W., Bohnenstiehl, D. R., Leithold, E., Osburn, C. L., &
50
51 714 Polyakov, V. 2013. Fingerprinting the sources of suspended sediment delivery
52
53 715 to a large municipal drinking water reservoir: Falls Lake, Neuse River, North
54
55 716 Carolina, USA. *Journal of Soils and Sediments*, 13(10), 1692–1707.
56
57
58
59
60

- 1
2
3 717 doi:10.1007/s11368-013-0758-3
4
5
6 718 Walling, D.E., Collins, A.L., & Stroud, R.W. 2008. Tracing suspended sediment and
7
8 719 particulate phosphorus sources in catchments. *Journal of Hydrology*, 350(3-4),
9
10 720 274–289. doi:10.1016/j.jhydrol.2007.10.047
11
12
13 721 Walling, D.E. 2013. The evolution of sediment source fingerprinting investigations in
14
15 722 fluvial systems. *Journal of Soils and Sediments*, 13(10), 1658-1675. doi:
16
17 723 10.1007/s11368-013-0767-2
18
19
20
21 724 Wasklewicz, T.A., Meek, N., 1995. Provenance of aeolian sediment: The upper
22
23 725 Coachella Valley, California. *Physical Geography* 16, 539-556.
24
25
26 726 Wilkinson, S.N., Hancock, G.J., Bartley, R., Hawdon, A.A., & Keen, R.J. (2013).
27
28 727 Using sediment tracing to assess processes and spatial patterns of erosion in
29
30 728 grazed rangelands, Burdekin River basin, Australia. *Agriculture, Ecosystems*
31
32 729 *and Environment*, 180, 90–102. doi:10.1016/j.agee.2012.02.002
33
34
35
36 730 Wilson, C.G., Papanicolaou, A.N.T., & Denn, K.D. (2012). Partitioning fine sediment
37
38 731 loads in a headwater system with intensive agriculture. *Journal of Soils and*
39
40 732 *Sediments*, 12(6), 966–981. doi:10.1007/s11368-012-0504-2
41
42
43 733 Winspear, N.R., Pye, K., 1996. Textural, geochemical and mineralogical evidence for
44
45 734 the sources of aeolian sand in central and southwestern Nebraska, USA.
46
47 735 *Sedimentary Geology* 101, 85-98.
48
49
50
51 736 Yang, X., Liu, Y., Li, C., Song, Y., Zhu, H., Jin, X., 2007. Rare earth elements of
52
53 737 aeolian deposits in Northern China and their implications for determining the
54
55 738 provenance of dust storms in Beijing. *Geomorphology* 87, 365-377.
56
57
58
59
60

1
2
3 739
4
5
6 740
7
8
9 741
10
11
12
13
14
15
16
17
18
19
20
21
22
23
24
25
26
27
28
29
30
31
32
33
34
35
36
37
38
39
40
41
42
43
44
45
46
47
48
49
50
51
52
53
54
55
56
57
58
59
60

For Peer Review

742 Tables

743 Table 1

	Grain size (μm)						
	<62.5	62.5 - 150	150 - 300	300 - 600	600 - 1180	1180 - 1700	
Mean Eocene marl (Egm) source (% $\pm 1\sigma$)	3.0 \pm 1.4	40.2 \pm 10.6	20.0 \pm 6	15.1 \pm 4.2	15.6 \pm 6.7	6.1 \pm 5	
Mean Quaternary clay flat (Qc) source (% $\pm 1\sigma$)	3.1 \pm 1.3	29.4 \pm 9.2	21.8 \pm 5.6	19.0 \pm 3.9	19.7 \pm 8.1	6.9 \pm 4	
Mean Quaternary terrace/fan (Qt2) source (% $\pm 1\sigma$)	2.2 \pm 2.3	34.7 \pm 7.3	20.4 \pm 5.6	17.1 \pm 3.9	19.3 \pm 5.3	6.4 \pm 2	
Mean Ashkzar erg dune sands (% \pm 1 σ)	1.1 \pm 0.9	47.8 \pm 9.3	29.7 \pm 8.4	17.4 \pm 13.9	3.4 \pm 5.4	0.6 \pm 1.3	
Ashkzar erg dune samples (%)	A	0.3	57.6	38.2	3.4	0.5	0.0
	B	0.5	41.0	18.1	39.0	1.4	0.0
	C	2.1	43.9	16.7	35.9	1.4	0.0
	D	0.5	42.5	34.0	22.0	1.0	0.0
	E	2.7	51.8	31.2	7.9	5.0	1.4
	F	1.0	64.5	32.0	2.5	0.0	0.0
	G	1.0	36.8	28.0	14.4	16.2	3.6
	H	0.6	44.6	39.3	13.7	1.8	0.0

744

745 Table 2

Fingerprint property	Chi square	p value	Fingerprint property	Chi square	p-value
La	6.669	0.036*	Y	4.151	0.125
Ce	7.476	0.024**	Zr	3.744	0.154
Pr	9.552	0.008**	Nb	0.582	0.748
Nd	0.415	0.813	Hf	16.1	<0.001***
Sm	0.081	0.96	Ta	4.922	0.085
Eu	10.23	0.006**	Th	10.28	0.006**
Gd	0.434	0.805	U	4.8	0.091
Tb	0.017	0.992	As	5.166	0.076
Dy	1.359	0.507	Bi	0.725	0.695
Ho	8.067	0.018*	Cd	0.111	0.946
Er	9.257	0.01*	Ga	13.4	<0.001***
Tm	8.373	0.015*	Ge	0.59	0.745
Yb	1.026	0.599	In	1.215	0.545
Lu	0.104	0.949	Li	7.213	0.027*
ΣREE	7.086	0.029*	Mo	0.227	0.893
Eu/Eu*	10.23	0.006**	P	13.05	<0.001***
(Nd/Yb)	0.785	0.675	S	16.36	<0.001***
(Gd/Yb) _n	0.729	0.695	Sb	1.409	0.494
(La/Yb) _n	13.89	0.001**	Se	0.858	0.651
(La/Sm) _n	4.725	0.094**	Sn	6.466	0.039*
(La/Lu) _n	12.78	0.002**	Te	4.685	0.096
δCe	5.435	0.041***	Ti	6.56	0.038*
Rb	15.18	<0.001***	Tl	6.614	0.037*
Sr	16.44	<0.001***	W	0.086	0.958
Ba	6.379	0.041*	Mn	1.673	0.433
V	3.083	0.214	Si	0.342	0.843
Cr	5.359	0.069	¹⁴³ Nd	1.042	0.534
Co	1.271	0.53	¹⁴⁴ Nd	2.031	0.362
Ni	3.998	0.135	⁸⁶ Sr	5.754	0.056
Cu	3.18	0.204	⁸⁷ Sr	7.124	0.028*
Zn	0.236	0.889			

746

747 Table 3

Sediment	Tracer	Optimum composite fingerprints					
		Rb	Sr	⁸⁷ Sr	(La/Yb) _n	Ga	δCe
Sand dune	Mean	7.8	144	85	7.1	1.2	0.69
	SD	0.74	18.6	28	0.54	0.11	0.020
Source	Tracer	Rb	Sr	⁸⁷ Sr	(La/Yb) _n	Ga	δCe
Egm	Mean	8.9	293	82	6.9	1.3	0.70
	SD	2.3	192	31	0.58	0.29	0.085
Qc	Mean	10	139	91	7.4	1.1	0.69
	SD	2.6	36.5	31	0.54	0.27	0.071
Qt2	Mean	7.1	163	98	7.7	0.99	0.74
	SD	0.82	135	44	0.89	0.26	0.27

748

749 Table 4

	Source	Tracer					
		Rb	Sr	⁸⁷ Sr	(La/Yb) _n	Ga	δCe
Raw data	Egm	0.944	0.362	0.930	0.996	0.980	0.810
	Qc	0.347	0.734	0.486	0.794	0.900	0.167
	Qt2	0.983	0.019	0.182	0.557	0.710	0.013
	Source	Rb	Sr	⁸⁷ Sr	(La/Yb) _n	Ga	δCe
Box-Cox transformed data	Egm	0.944	0.724	0.930	0.996	0.980	0.978
	Qc	0.347	0.931	0.486	0.794	0.900	0.542
	Qt2	0.983	0.085	0.182	0.557	0.710	0.061

750

751 Table 5

752

Sediment samples	Source	Mean (%)	SD (%)	MC error	Median	Percentile (2.5)	Percentile (97.5)
A	Egm	44.1	11.5	0.003	44.5	21	64.7
	Qc	39.8	11.2	0.003	37.9	22.7	65.8
	Qt2	16.2	8.3	0.001	15.2	3.6	34
B	Egm	32.6	7.3	0.002	33	18.2	46.2
	Qc	5.1	3.8	0.001	4.1	0.6	15
	Qt2	62.2	6	0.001	62.1	50.3	73.7
C	Egm	20.8	6.3	0.002	21	8.1	33
	Qc	27.5	6.5	0.002	26.6	17.1	43
	Qt2	51.6	5.2	0.000	51.1	42	62.5
D	Egm	56.3	13	0.004	56.9	29.9	79.4
	Qc	28.7	10.5	0.003	27	12.2	53.4
	Qt2	14.9	9.4	0.001	14.4	0.4	34.2
E	Egm	14.3	5	0.001	14.3	4.6	24.6

		Qc	23	5.3	0.001	22.3	14.2	35.1
		Qt2	62.6	4.8	0.000	62.7	52	71.9
	F	Egm	17.6	6.3	0.001	17.7	4.8	29.9
		Qc	32.4	7.4	0.002	31.5	20.4	49.6
		Qt2	49.9	5.5	0.001	49.4	39.7	61.5
	G	Egm	3.4	3.2	0.000	2.44	0.000	12.2
		Qc	3.9	3.9	0.000	2.6	0.000	14.7
		Qt2	92.7	6	0.001	94	78.2	99.7
	H	Egm	37.3	11.2	0.003	37.8	14.5	57.9
		Qc	49.7	12.6	0.004	47.7	30	79
		Qt2	13	8.6	0.001	12	0.4	31.5

753

754

For Peer Review

1
2
3 755 Figure captions
4
5

6 756
7

8 757 *Figure 1: Location and geological map of the Yazd-Ardekan Plain and sampling*
9
10 758 *sites. Dominant and minor wind directions shown in Part C. Number of sampling*
11
12 759 *points = 57. Qt2, Qc, Egm (potential sediment sources) and Qsd (sediment)*
13
14 760 *represent young alluvial fans and terraces, clay flats, gypsiferous marl and sand*
15
16 761 *dunes, respectively.*
17

18
19 762
20

21 763 *Figure 2: Source and sediment sink regions within the study area. Source regions*
22
23 764 *include: a) clay flats (Qc); b) gypsiferous marl (Egm); and c) young alluvial fans and*
24
25 765 *terraces (Qt2). Sediment sinks include: d) sand dunes (Qsd).*
26
27

28 766
29

30 767 *Figure 3. Morphological mapping of dune types within Ashkzar erg reveals the*
31
32 768 *dominance of barchans and barchanoid ridges. There are less distinct zones within*
33
34 769 *the dunefield in the north, where the interdunes are sandy and the transverse forms*
35
36 770 *much less distinct, and in the far southeast, where patchy slipface-less dunes*
37
38 771 *dominate. Base imagery is courtesy of Google Earth™, and letters refer to the eight*
39
40 772 *samples analysed for physical and geochemical characteristics within the dunefield.*
41
42

43 773
44

45 774 *Figure 4: A directed acyclic graph of the Bayesian mixing model employed in this*
46
47 775 *study.*
48

49 776
50

51
52 777 *Figure 5: Two-dimensional scatter plot of the first and second discriminant functions*
53
54 778 *from stepwise DFA for the source groups Egm (Eocene gypsiferous marls), Qc*
55
56 779 *(Quaternary clay flats) and Qt2 (Quaternary alluvial fans and terraces).*
57
58
59
60

1
2
3 780 *Figure 6: Source contributions for each aeolian sediment samples by Bayesian*
4
5 781 *mixing model with 95% credible limits. Base imagery is courtesy of Google Earth™.*
6
7

8 782
9

10
11 783 Table captions
12

13
14 784 *Table 1: Grain size data for the source areas, the dunefield, and individual samples*
15
16 785 *from within the dunefield.*
17

18
19 786
20

21 787 *Table 2: Kruskal-Wallis H test results for selecting fingerprint properties for*
22
23 788 *distinguishing individual source types. Confidence is highlighted at >95% with a*
24
25 789 *single asterisk, >99% with a double asterisk, and >99.9% with a triple asterisk.*
26

27
28 790
29

30 791 *Table 3: Summary geochemistry data for sand dune samples and potential sediment*
31
32 792 *sources. All are reported to two significant figures, except Sr, which is reported to*
33
34 793 *three, due to the larger magnitude of the concentrations.*
35

36
37 794
38

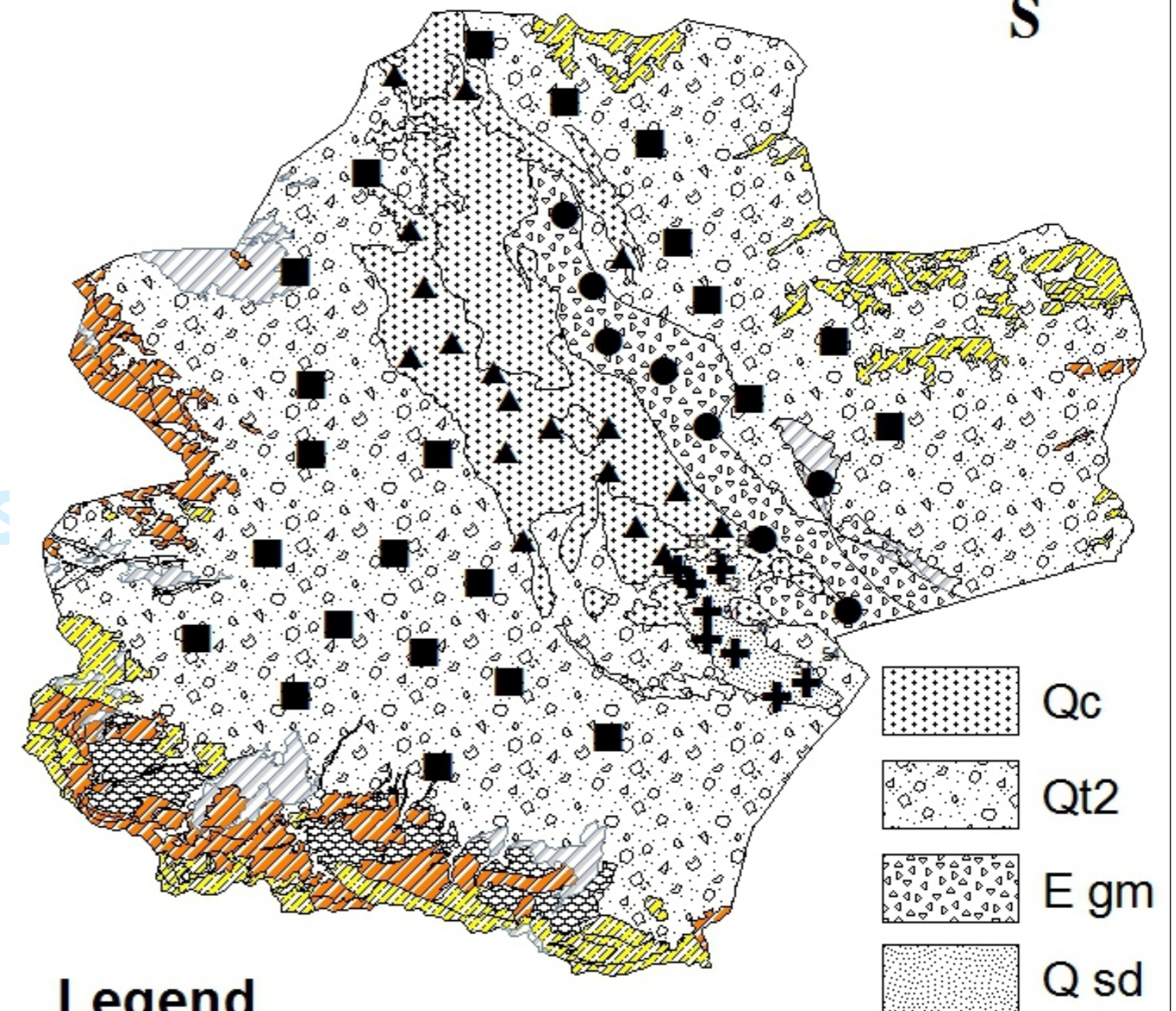
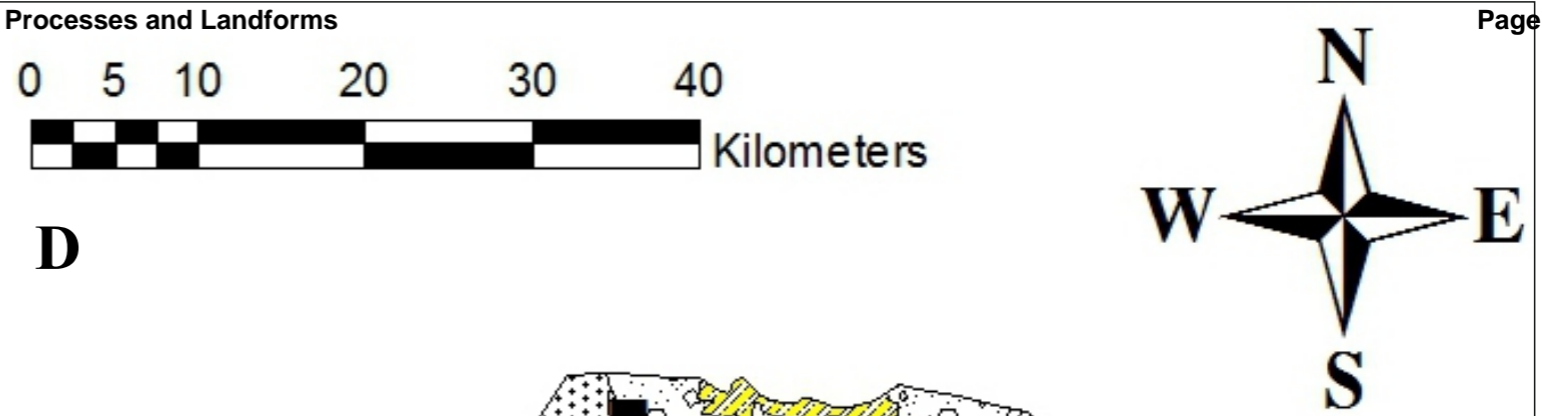
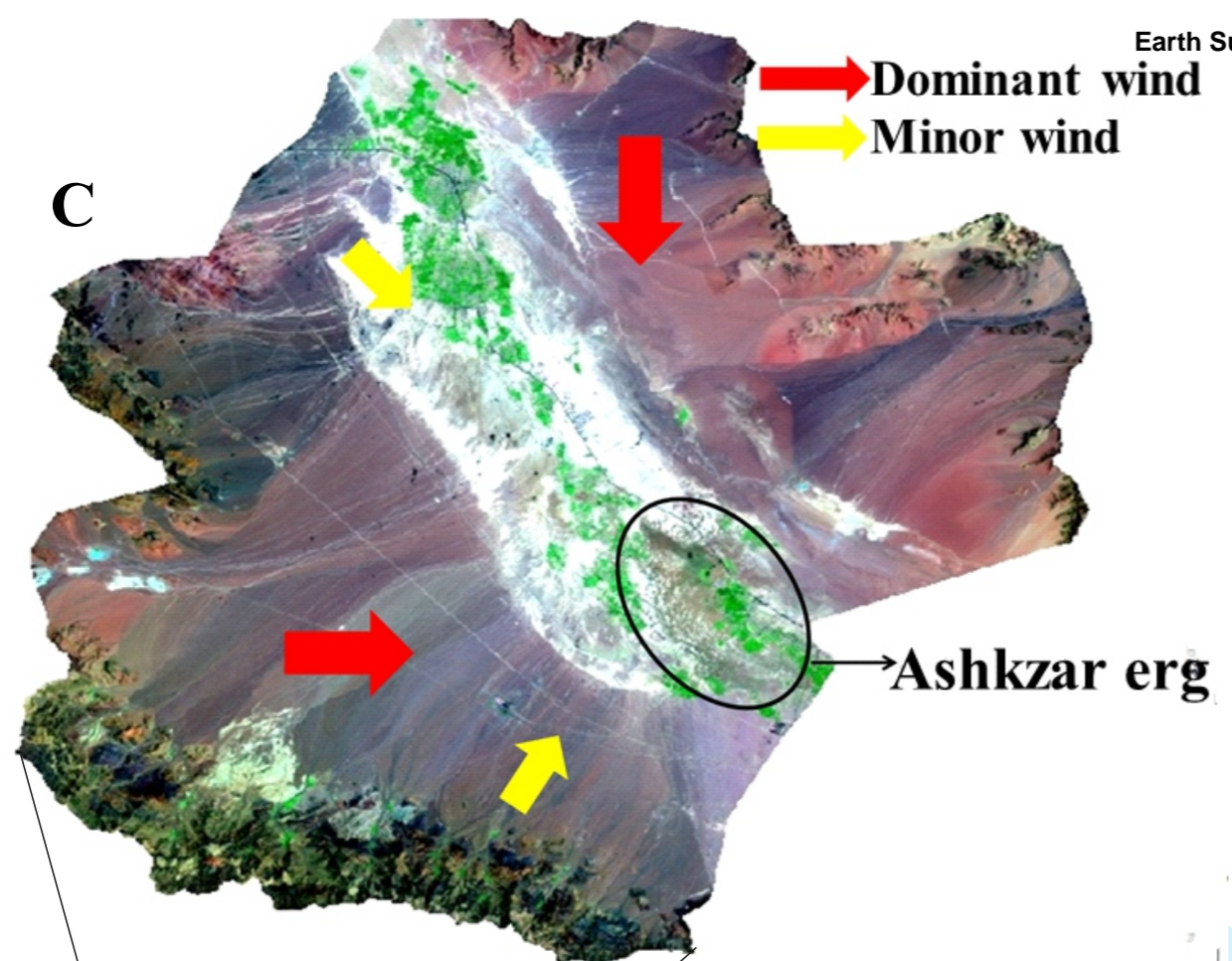
39 795 *Table 4: Normality tests on the raw data for the tracers selected for the fingerprint*
40
41 796 *revealed that two tracers (Sr and $\delta^{13}C$) were not normally distributed for the Qt2 unit;*
42
43 797 *for this reason, Box-Cox transformations were performed on all data, which did*
44
45 798 *provide normal distributions for all tracers.*
46

47
48 799
49

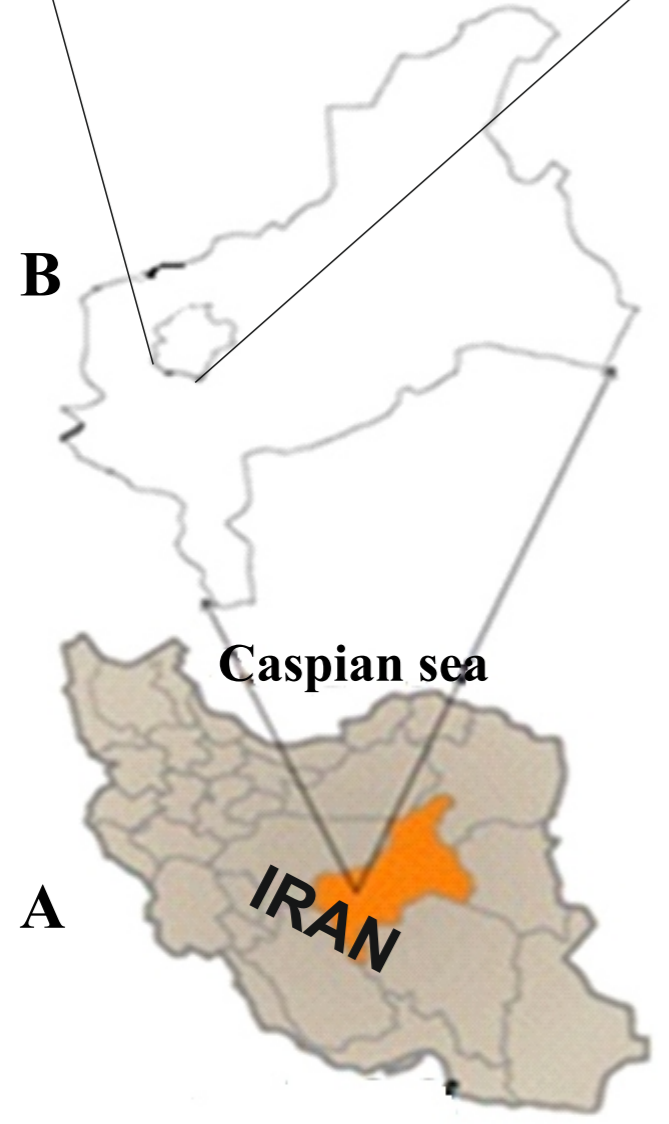
50 800 *Table 5. Estimated contribution from each source for aeolian sediment samples by*
51
52 801 *Bayesian mixing model.*
53

54
55 802
56

57 803
58
59
60



A. Iran map
B. Yazd Province boundary
C. Satellite image of Yazd-Ardekan Plain
D. Geological map of Yazd-Ardekan Plain

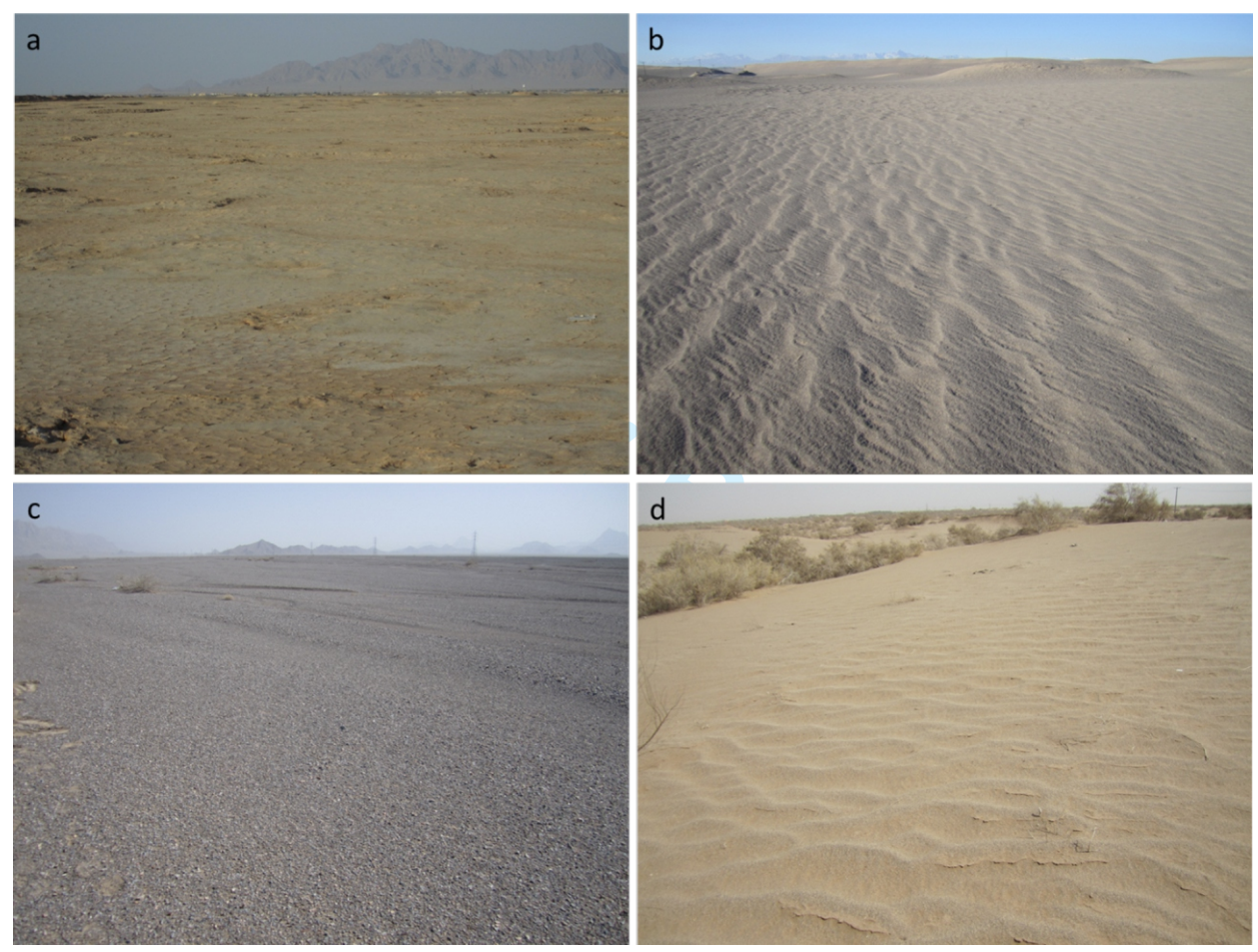


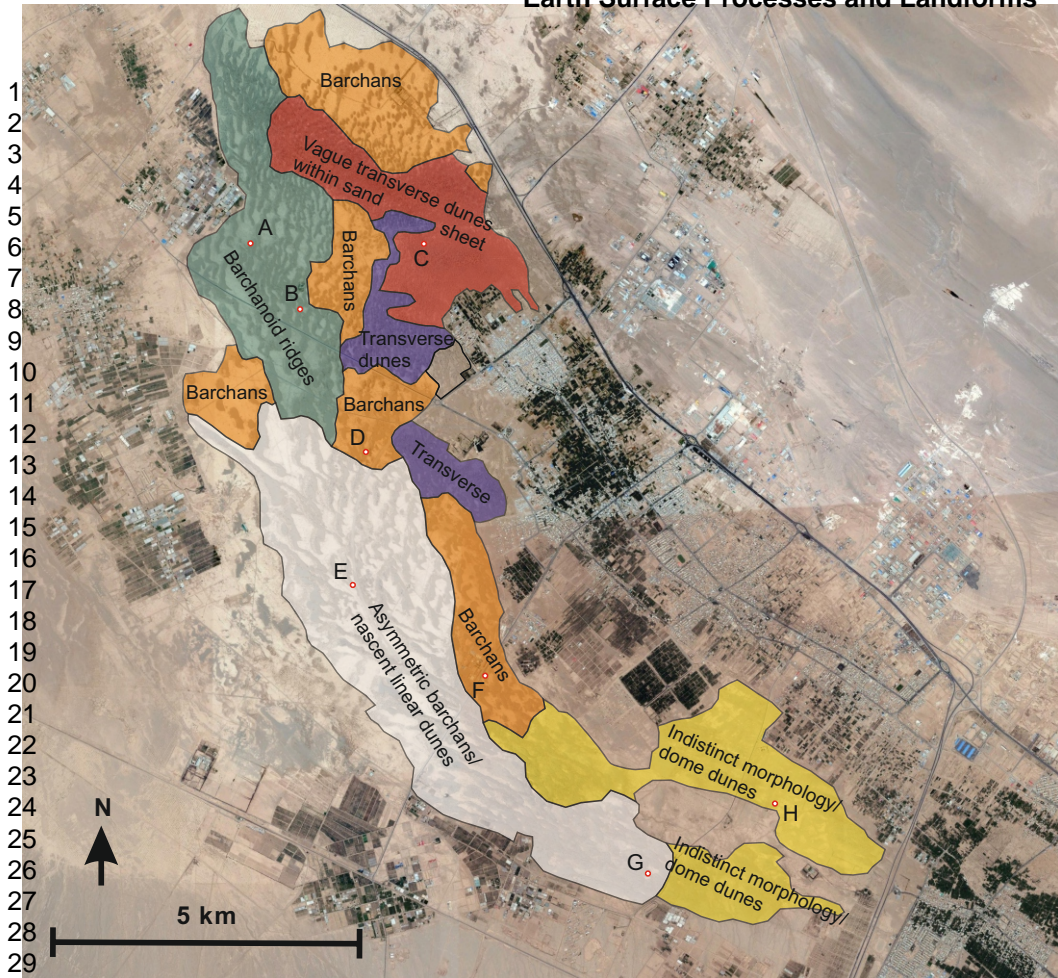
Legend

- Egm sample
- Qt2 sample
- ▲ Qc sample
- ✚ Sand dune sample
- ▨ Paleozoic Formations
- ▧ Cenozoic Formations
- ▩ Mesozoic Formations
- ▤ Pre-Cambrian Formations
- ▧ Qc
- ▨ Qt2
- ▩ E gm
- ▤ Q sd

1
2
3
4
5
6
7
8
9
10
11
12
13
14
15
16
17
18
19
20
21
22
23
24
25
26
27
28
29
30
31
32
33
34
35
36
37
38
39
40
41
42
43
44
45
46
47
48
49
50
51
52
53
54
55
56
57
58
59
60

1
2
3
4
5
6
7
8
9
10
11
12
13
14
15
16
17
18
19
20
21
22
23
24
25
26
27
28
29
30
31
32
33
34
35
36
37
38
39
40
41
42
43
44
45
46
47





Peer Review

1
2
3
4
5
6
7
8
9
10
11
12
13
14
15
16
17
18
19
20
21
22
23
24
25
26
27
28
29
30
31
32
33
34
35
36
37
38
39
40
41
42
43
44
45
46
47
48
49
50
51
52
53
54
55
56
57
58
59
60

1
2
3
4
5
6
7
8
9
10
11
12
13
14
15
16
17
18
19
20
21
22
23
24
25
26
27
28
29
30
31
32
33
34
35
36
37
38
39
40
41
42
43
44
45
46
47
48
49
50
51
52
53
54
55
56
57
58
59
60

Source

Contribution

Sediment

